

Energy & Environmental Science

Suppressed Non-Radiative Loss and Efficient Hole Transfer at Small Highest Occupied Molecular Orbital Offset Enables 19.73% Efficiency Binary Organic Solar Cells with Small Efficiency-Cost Gap

Laboratory of Organi Li, Zhenyu; Zhengzh Li, Xinrui; Zhengzho Wu, Yilei; Stanford U Sun, Rui; Wuhan Un	zhou University
Date Submitted by the Author: Complete List of Authors: Kong, Xiaolei; Zheng Yang, Nana; Zhengz Zhang, Xixi; Zhengz Zhang, Jinyuan; Inst Laboratory of Organi Li, Zhenyu; Zhengzh Li, Xinrui; Zhengzho Wu, Yilei; Stanford L Sun, Rui; Wuhan Un	
Author: Complete List of Authors: Kong, Xiaolei; Zheng Yang, Nana; Zhengz Zhang, Xixi; Zhengz Zhang, Jinyuan; Inst Laboratory of Organi Li, Zhenyu; Zhengzh Li, Xinrui; Zhengzho Wu, Yilei; Stanford L Sun, Rui; Wuhan Un	
Yang, Nana; Zhengz Zhang, Xixi; Zhengz Zhang, Jinyuan; Inst Laboratory of Organi Li, Zhenyu; Zhengzh Li, Xinrui; Zhengzho Wu, Yilei; Stanford U Sun, Rui; Wuhan Un	
Sciences Li, Aoxiang; Zhengzh Min, Jie; Wuhan Univ Yang, Guang; Zheng Sun, Chenkai; Zheng	nou University itute of Chemistry Chinese Academy of Sciences, c Solids ou University u University niversity, Department of Chemical Engineering versity stitute of Physics and Chemistry Chinese Academy of

SCHOLARONE™ Manuscripts

Broader context

Organic solar cell (OSC) is a promising next-generation photovoltaic technology due to the advantages of solution processability, light weight, and promise in manufacturing large-scale flexible devices. However, most of the reported high-performance OSCs are based on the wide bandgap conjugated polymer donors with complex chemical structures, tedious multi-step synthesis, multiple purifications, and low total synthetic yields. Therefore, it is urgent to focus on those low-cost polymer donors to realize a "win-win" situation of material cost and photovoltaic performance of OSCs for industrialization. Herein, two novel A-DA'D-A type small molecule acceptors (SMAs) with different conjugated outer side chains are designed and synthesized to explore the potential of low-cost polymer donor PTQ11 and pursue the small efficiency-cost gap OSCs for industrialization. Eventually, the OSCs based on PTQ11 and PEH-F realize the highest efficiency of OSCs based on the low-cost polymers and the lowest estimated minimum sustainable price so far, implying that PTQ11:PEH-F binary system is a promising candidate with small efficiency-cost gap for industrial organic photovoltaic. Overall, the methodology for calculating the cost of solar modules and the superior results delivered by this work will provide important insights into the process of development and commercialization in the field of organic photovoltaics.

ARTICLE

Received 00th January 20xx, Accepted 00th January 20xx

DOI: 10.1039/x0xx000000x

Suppressed Non-Radiative Loss and Efficient Hole Transfer at Small Highest Occupied Molecular Orbital Offset Enables 19.73% Efficiency Binary Organic Solar Cells with Small Efficiency-Cost Gap

Xiaolei Kong, ‡*a Nana Yang, ‡a Xixi Zhang, a Jinyuan Zhang, b Zhenyu Li, a Xinrui Li, a Yilei Wu, c Rui Sun, d Jing Li, a Aoxiang Li, a Jie Min, d Guang Yang, a and Chenkai Sun*a

Suppressing energy/voltage loss and realizing efficient charge transfer at small frontier molecular orbital offsets between donor and acceptor is viable to simultaneously improve open-circuit voltage (V_{oc}) and short-circuit current (J_{sc}), and thus power conversion efficiency (PCE) of organic solar cells (OSCs). Here, two A-DA'D-A type acceptors, PEH-F and TEH-F, are designed and synthesized with different conjugated outer side chains, to pursue high-efficiency and cost-effective OSCs for industrialization. In comparison with TEH-F (thienyl outer side chain), PEH-F with phenyl outer side chains delivers up-shifted frontier energy levels, wider optical bandgap, and higher absorption coefficient. By adopting low-cost polymer PTQ11 as donor, the PEH-F-based device realizes low energy loss of 0.511 eV with suppressed non-radiative loss of only 0.182 eV, and exhibits efficient exciton dissociation and hole transfer even at an extremely small highest occupied molecular orbital offset of 0.06 eV. Eventually, the PTQ11:PEH-F-based binary device demonstrates a superior PCE of 19.73 % with high V_{oc} and J_{sc} simultaneously, which is the highest PCE to date for OSCs based on low-cost polymer donors. More importantly, this device shows small efficiency-cost gap for industrialization with the estimated minimum sustainable price (MSP) of 0.35 \$ W_p-1, which is dramatically lower than other reported high-performance OSCs.

Introduction

Organic solar cells (OSCs), with a blend photoactive layer of a *p*-type conjugated polymer as donor and an *n*-type organic semiconductor as acceptor, have attracted great attentions in the past several decades owing to their unique features such as low-cost fabrication by solution processing, mechanical flexibility, light weight, and large-scale applications.^{1–8} Due to the significant innovations in efficient photovoltaic materials,^{9–17} interface buffer layer materials,^{18–21} and device engineering,^{22–25} especially the invention of A-DA'D-A type small molecule acceptors (SMAs),^{13–15,26} the power conversion efficiency (PCE) of the state-of-the-art single-junction OSCs has reached over 19%, satisfying the requirement of photovoltaic performance for industrialization.

Nowadays, most of the reported high-performance OSCs

are based on the wide bandgap conjugated polymer donors, such as PM6, 9 D18, 11 and D18-Cl, 12 etc., which possess excellent photovoltaic properties. However, due to the complex chemical structures, tedious multi-step synthesis, multiple purifications, and low total synthetic yields, the costs of those polymer donors are too high to enable large-scale preparation and industrial application.^{27,28} Therefore, it is urgent to focus on those lowcost polymer donors to realize a "win-win" situation of material cost and photovoltaic performance of OSCs for industrialization. PTQ10,¹⁰ a classic low-cost polymer donor, possesses simple molecular structure, low energy disorder, and great uniform vertical phase distribution, as well as benefiting from the developments of A-DA'D-A type SMAs, thus enabling PTQ10based single-junction OSCs have achieved outstanding PCEs exceeding 19%.^{29,30} However, the PCEs of OSCs based on another low-cost polymer donor PTQ11 (see Fig. 1a, a derivative of PTQ10 with methyl substituent on its quinoxaline unit) have so far remained around 16%, despite the fact that PTQ11 has stronger molecular crystallinity and better charge transport capability than PTQ10.31 Therefore, there is a great potential for PTQ11 that has not yet been explored.

On the other hand, the high voltage/energy loss ($V_{\rm loss}/E_{\rm loss}$) of OSCs resulting from the small dielectric constant and large exciton binding energy of organic photovoltaic materials is the key issue that leads to their current PCEs dramatically lower than that of inorganic and perovskite solar cells. $^{32-35}$ For the classical OSCs with a blended donor and acceptor photoactive layer, the feasible strategy to increase the open-circuit voltage ($V_{\rm oc}$) and reduce the $V_{\rm loss}/E_{\rm loss}$ is to up-shift the lowest

^{a.} College of Chemistry, Zhengzhou University, Zhengzhou 450001, China.

b. Beijing National Laboratory for Molecular Sciences, CAS Key Laboratory of Organic Solids, Institute of Chemistry, Chinese Academy of Sciences, Beijing 100190, China.

^c Department of Chemistry, Stanford University, Stanford, California 94305-4125, United States.

^{d.} The Institute for Advanced Studies, Wuhan University, Wuhan 430072, China.

^e Key Laboratory of Photochemical Conversion and Optoelectronic Materials, Technical Institute of Physics and Chemistry, Chinese Academy of Sciences, Beijing 100190, China.

[†] Electronic supplementary information (ESI) available Sec DOI: 10.1039/x0xx00000x

[‡] X. K. and N. Y. contributed equally to this work. E-mail: xlkong@zzu.edu.cn; schenkai@zzu.edu.cn

unoccupied molecular orbital (LUMO) energy level (E_{LUMO}) of acceptor or/and down-shift the highest occupied molecular orbital (HOMO) energy level (E_{HOMO}) of donor, and thus broadening the frontier orbital energy offset ($\Delta E_{LUMO(A)-HOMO(D)}$). $^{36-38}$ However, enlarging the $\Delta E_{LUMO(A)-HOMO(D)}$ will certainly bring about a decrease in $\Delta E_{HOMO(D-A)}$ or/and $\Delta E_{LUMO(D-A)}$, which in turn leads to a reduced driving force for the exciton dissociation and charge transfer (CT), thus resulting in the restricted charge generation and the limited photogenerated current in OSCs. 39,40 Therefore, fine tuning the molecular structure of organic photovoltaic materials to realize effective exciton dissociation and CT at low V_{loss}/E_{loss} , to maximize the open-circuit voltage (V_{oc}) and short-circuit current density (J_{sc}) of the devices simultaneously, is crucial to further improve the PCE of OSCs.

On the basis of previous works, it seems that the PTQ derivative donors prefer to match with the A-DA'D-A type SMAs with bulky conjugated outer side chains for high-performance OSCs.^{29,30,41–44} Hence, we designed and synthesized two novel

A-DA'D-A type SMAs with different conjugated outer side chains in this work, namely PEH-F and TEH-F (their molecular structures are shown in Fig. 1a), to explore the potential of lowcost polymer donor PTQ11 and pursue the small efficiency-cost gap OSCs for industrialization. Eventually, benefiting from the low E_{loss} of 0.511 eV with suppressed non-radiative loss of only 0.182 eV, and efficient exciton dissociation and hole transfer processes even at an extremely small $\Delta E_{\text{HOMO(D-A)}}$ of 0.06 eV, the PTQ11:PEH-F-based binary device achieves a remarkable PCE of 19.73% with a high $V_{\rm oc}$ of 0.936 V and a large $J_{\rm sc}$ of 26.53 mA cm⁻ ² simultaneously. To the best of our knowledge, 19.73% is the highest PCE ever achieved for OSCs based on low-cost polymer donors. More importantly, PTQ11:PEH-F-based device shows small efficiency-cost gap for industrialization with the estimated minimum sustainable price (MSP) of only 0.35 \$ W_p-1, which is dramatically lower than other reported high-performance OSCs. These results implying that the PTQ11:PEH-F binary system is a promising candidate with small efficiency-cost gap for large-area fabrication and industrial applications of OSCs.

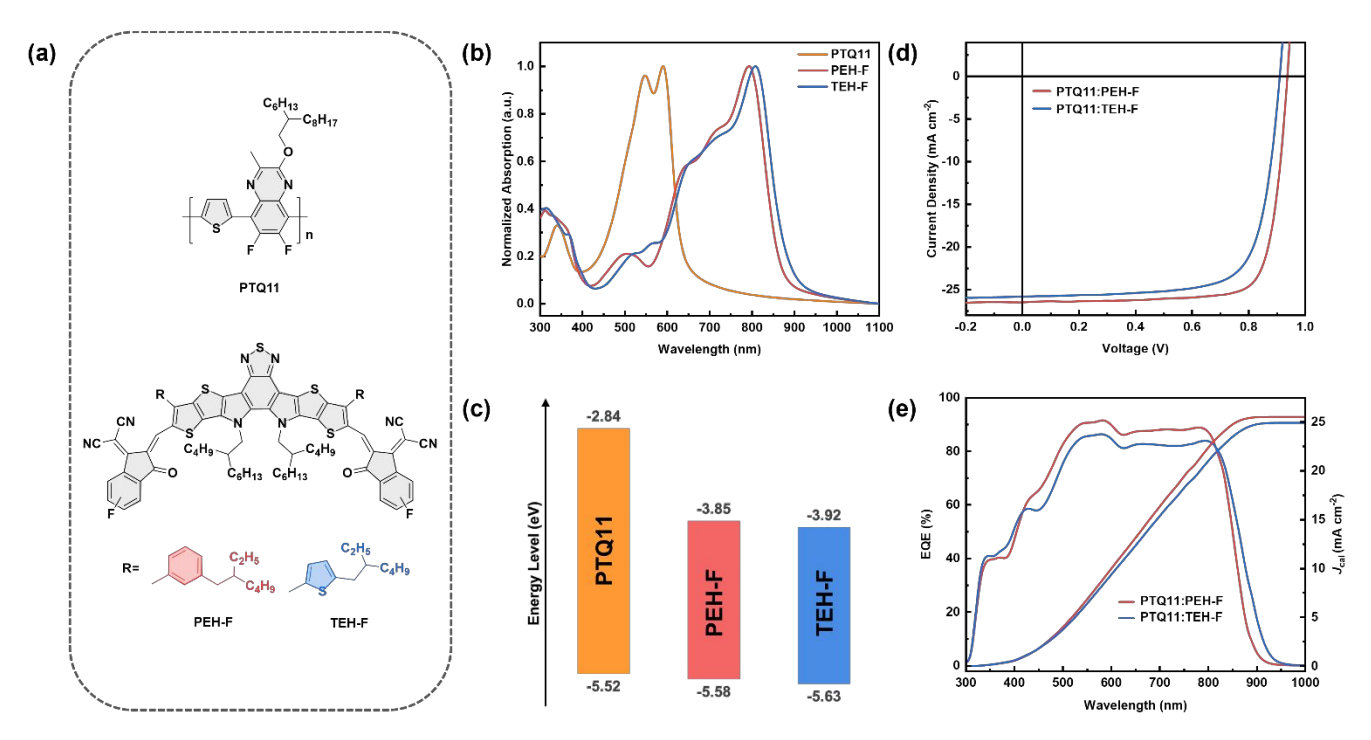


Fig. 1 (a) Molecular structures of the polymer donor PTQ11, and two SMAs, PEH-F and TEH-F. (b) Normalized UV-vis absorption spectra of the donor and SMAs films. (c) Energy level diagram of the donor and SMAs. (d) *J-V* curves of the optimized OSCs based on PTQ11:SMA under the illumination of AM 1.5G, 100 mW cm⁻². (e) EQE spectra of the corresponding optimized OSCs.

Results and Discussion

Molecular Synthesis and Characterization

Fig. 1a shows the molecular structures of polymer donor PTQ11 and two SMAs PEH-F and TEH-F, and the detailed synthetic routes of two SMAs are depicted in Scheme S1 and S2 in the electronic supplementary information (ESI). It is worth noting that the monofluorine-substituted end group is used for constructing two SMAs instead of the most widely used

bifluorine-substituted end group because of its lower cost and weaker electron-withdrawing property to realize higher E_{LUMO} of two SMAs for achieving higher V_{oc} in the devices. Based on the synthetic process and isolation/purification process in combination with the dosage and price of raw compounds, intermediates, reagents, synthetic yield of each chemical reactions, and the isolation/purification operations (more detailed description as depicted in the "Cost Feasibility of Organic Photovoltaic Materials" section of ESI), the cost-per-kilogram (C_{kg}) is calculated to be 234.74 \times 10³ \$ kg¹ and 234.72

 \times 10³ \$ kg⁻¹ for PEH-F and TEH-F respectively, lower than that of their analogues m-PEH (264.46 \times 10³ \$ kg⁻¹) and o-TEH $(264.44 \times 10^3 \text{ $kg}^{-1})$ with bifluorine-substituted end groups reported in our previous work (the specific calculations are summarized in Table S1-S4 and S14).^{29,42} The number average molecular weight (M_n) of PTQ11 was measured to be 47.3 kDa with appropriate polydispersity index (PDI) of 2.51 by the hightemperature gel-permeation chromatography (GPC), as shown in Fig. S1 in the ESI. PTQ11 and two SMAs all exhibit good thermal stability with thermal decomposition temperature (T_d) at 5% weight loss of 380 °C for PTQ11, 311 °C for PEH-F, and 314 °C for TEH-F, respectively (as illustrated in Fig. S2), which are high enough for the application as photovoltaic materials in OSCs. Fig. 1b and Fig. S3b displays the normalized ultravioletvisible (UV-vis) absorption spectra of PTQ11, PEH-F, and TEH-F in thin films, and Fig. S3a shows the absorption spectra of PTQ11:PEH-F and PTQ11:TEH-F blends in chloroform solutions and thin films. The corresponding optical data of two SMAs are summarized in Table 1. PEH-F and TEH-F films show similar absorption profiles ranging from 300 to 1000 nm, and their maximum absorption peaks are located at 793 and 808 nm with absorption coefficients of 1.26×10^5 and 1.09×10^5 cm⁻¹, respectively. Compared with PEH-F, the TEH-F film possesses

red-shifted and broadened absorption profile, which may be related with their molecular geometry and aggregation properties. The optical bandgap ($E_{\rm g}^{\rm opt}$) of TEH-F is measured to be 1.40 eV and slightly narrower than that of PEH-F (1.42 eV). Since the absorption region of PTQ11 film is mainly located in the range from 400 to 700 nm, both SMAs show complementary absorption with PTQ11 in the visible to infrared region, which could potentially provide wide and efficient absorption to obtain higher $J_{\rm sc}$ in the devices.

The electronic energy levels of PTQ11, PEH-F, and TEH-F are determined by cyclic voltammetry (CV) measurement based on their redox potentials (Fig. S4). Then the $E_{\rm HOMO}/E_{\rm LUMO}$ values of PTQ11, PEH-F, and TEH-F are calculated to be -5.52/-2.84 eV, -5.58/-3.85 eV, and -5.63/-3.92 eV, respectively (as shown in Table 1 and Fig. 1c). Since the $V_{\rm oc}$ of OSCs depends on the difference between the $E_{\rm LUMO(A)}$ and the $E_{\rm HOMO(D)}$, the up-shifted $E_{\rm LUMO}$ of PEH-F could contribute to a higher $V_{\rm oc}$ in OSCs than that of TEH-F-based device. However, achieving efficient exciton dissociation and hole transfer may be a huge challenge in the PTQ11:PEH-F blend due to its extremely small $\Delta E_{\rm HOMO(D-A)}$ of only 0.06 eV between donor PTQ11 and acceptor PEH-F.

Table 1 The physicochemical properties of PEH-F and TEH-F.

Acceptors	λ _{max, film} (nm)	λ _{onset, film} (nm)	$oldsymbol{arepsilon_{film}}$ ($10^5 ext{cm}^{ ext{-}1}$)	$E_{ m g}^{ m opt}$ (eV) a	Е_{номо}/Е_{гимо} (eV) ^b
PEH-F	793	873	1.26	1.42	-5.58/-3.85
TEH-F	808	888	1.09	1.40	-5.63/-3.92

 $[^]a$ Calculated from the onset absorption of thin films: E_g^{opt} = 1240/ λ_{onset} .

Photovoltaic Performances

In order to assess the photovoltaic performance of PEH-F and TEH-F, the OSCs are fabricated with PTQ11 as donor and with a conventional device structure of ITO/ 2PACz/PTQ11:SMA/PFN-Br/Ag. Fig. 1d shows the current density-voltage (J-V) characteristics of the optimized OSCs, and Table 2 lists the detailed photovoltaic performance parameters for a clear comparison. In addition, box plots and normal distribution curves for each performance parameter from sixteen individual devices based on PTQ11:PEH-F or PTQ11:TEH-F are illustrated in Fig. S5, respectively. As mentioned above, there is usually a competition between high $V_{\rm oc}$ and high $J_{\rm sc}$ in OSCs, that is, achieving both high $V_{\rm oc}$ and $J_{\rm sc}$ in OSCs is a huge challenge. However, the PTQ11:PEH-F-based device realizes a high $V_{\rm oc}$ of 0.936 V and a large $J_{\rm sc}$ of 26.53 mA cm⁻² simultaneously, coupled with a high fill factor (FF) of 79.45%, ultimately resulting in a

superior PCE of 19.73%, which indicates that the device could successfully deliver low V_{loss}/E_{loss} , effective exciton dissociation and CT at the same time. As far as we know, 19.73% is the highest PCE reported to date for OSCs based on the low-cost polymers. In contrast, the OSCs based on PTQ11:TEH-F demonstrate a poor PCE of 17.40%, with a $V_{\rm oc}$ of 0.909 V, a $J_{\rm sc}$ of 25.85 mA cm⁻², and a FF of 74.05%. Fig. 1e displays the external quantum efficiency (EQE) spectra of the optimal OSCs, and Fig. S6 exhibits the EQE spectra of five individual devices based on PTQ11:PEH-F or PTQ11:TEH-F, respectively. In the wavelength range from 450 nm to 850 nm, the OSC based on PTQ11:PEH-F displays much stronger photo-to-electron response, and therefore obtains a higher calculated J_{sc} (J_{cal}) value (25.52 mA cm⁻²) than that (24.92 mA cm⁻²) of PTQ11:TEH-F-based device, which agrees quite well with the trend of J-V characteristics within 4% mismatch.

^b Calculated from the onset of reduction/oxidation potentials.

Table 2 Photovoltaic performance parameters of the optimal OSCs based on PTQ11:SMA, under illumination of AM 1.5G (100 mW cm⁻²).

Active layers	$oldsymbol{V_{oc}}$ (V) a	$J_{\rm sc}$ (mA cm ⁻²) a	FF (%) ^a	PCE (%) ^a
PTQ11:PEH-F	0.936	26.53	79.45	19.73
	(0.933±0.003)	(26.67±0.19)	(78.78±0.36)	(19.60±0.15)
PTQ11:TEH-F	0.909	25.85	74.05	17.40
	(0.908±0.003)	(25.67±0.20)	(73.71±0.58)	(17.19±0.16)

^a The statistical values in the brackets are obtained from sixteen different devices.

Voltage/Energy Loss Analysis

How to suppress V_{loss}/E_{loss} and thus maximize V_{oc} by rational molecular design is the key point of achieving highperformance OSCs but still confronts a great challenge. 36,35,40 According to the J-V photovoltaic performance parameters, both PTQ11:PEH-F and PTQ11:TEH-F systems exhibit high $V_{\rm oc}$ over 0.9 V. Firstly, it could be related to the up-shifted E_{LUMO} of two acceptors caused by the utilization of the monofluorinesubstituted terminal groups with relatively weaker electronwithdrawing feature. Moreover, we consider that the more profound reason may be attributed to the low V_{loss}/E_{loss} of two systems. Therefore, to gain further insight into the high $V_{
m oc}$ obtained in PEH-F/TEH-F systems, the V_{loss}/E_{loss} details in both devices have been measured (the corresponding results have been summarized in Fig. 2, Fig. S7 and Table S16). Based on the Shockley-Queisser (SQ) limit, the V_{loss}/E_{loss} in OSCs can be divided into three parts (Fig. 2a), as shown in following equation (1):45

$$E_{\text{loss}} = qV_{\text{loss}} = E_{\text{g}} - qV_{\text{oc}}$$

$$= (E_{\text{g}} - qV_{\text{oc}}^{\text{SQ}}) + (qV_{\text{oc}}^{\text{SQ}} - qV_{\text{oc}}^{\text{rad}}) + (qV_{\text{oc}}^{\text{rad}} - qV_{\text{oc}})$$

$$= (E_{\text{g}} - qV_{\text{oc}}^{\text{SQ}}) + q\Delta V_{\text{oc}}^{\text{rad,below gap}} + q\Delta V_{\text{oc}}^{\text{non-rad}}$$

$$= \Delta E_{1} + \Delta E_{2} + \Delta E_{3} \qquad (1)$$

For ΔE_1 , it is the inevitable radiative recombination loss for all types of solar cells and derives from the mismatch between AM 1.5G spectrum and black body spectrum above the optical bandgap. The ΔE_1 for both systems are close (~ 0.260 eV) because of their similar optical bandgaps. For ΔE_2 , it is the

additional radiative recombination loss caused by the non-step absorption of photoactive blend (0.069 eV for PTQ11:PEH-F-based OSCs and 0.036 eV for PTQ11:TEH-F-based OSCs), which is related to their energy disorder at the tail-state absorption. Generally, the degree of energy disorder could be quantified by a parameter of Urbach energy ($E_{\rm U}$), and the relationship between tail-state absorption $\alpha(E)$ and $E_{\rm U}$ follows the Urbach rule expressed as follows:³⁴

$$\alpha(E) = \alpha_0 e^{\frac{(E - E_0)}{E_U}} \tag{2}$$

Where, α_0 and E_0 are two constants, and E is the photon energy. Thus, the smaller E_U represents the lower degree of energy disorder. By measuring the high-resolution Fourier transform photocurrent spectroscopy EQE spectra (FTPS-EQE), we are able to derive E_U values through exponential fitting, which are 22.9 meV for PTQ11:PEH-F-based OSCs and 21.3 meV for PTQ11:TEH-F-based OSCs (as shown in Fig. 2d). The variation of E_U is consistent with that of ΔE_2 , and the effects of energetic disorder reduction on the ΔE_2 in devices are confirmed.⁴⁶ Then for ΔE_3 , it is the nonradiative recombination loss and large ΔE_3 is considered to be the main drawback that causes OSCs to lag behind the other high-performance photovoltaics.^{47,48} Impressively, the devices based on PTQ11:PEH-F exhibit a remarkable ΔE_3 value of only 0.182 eV, while the ΔE_3 value for PTQ11:TEH-F-based devices is 0.219 eV. Eventually, both two systems offer low E_{loss} values of 0.511 eV for PTQ11:PEH-F-based device and 0.513 eV for PTQ11:TEH-Fbased device, which should be the underlying rationale for the $V_{\rm oc}$ values of both two systems to be higher than 0.9 V.

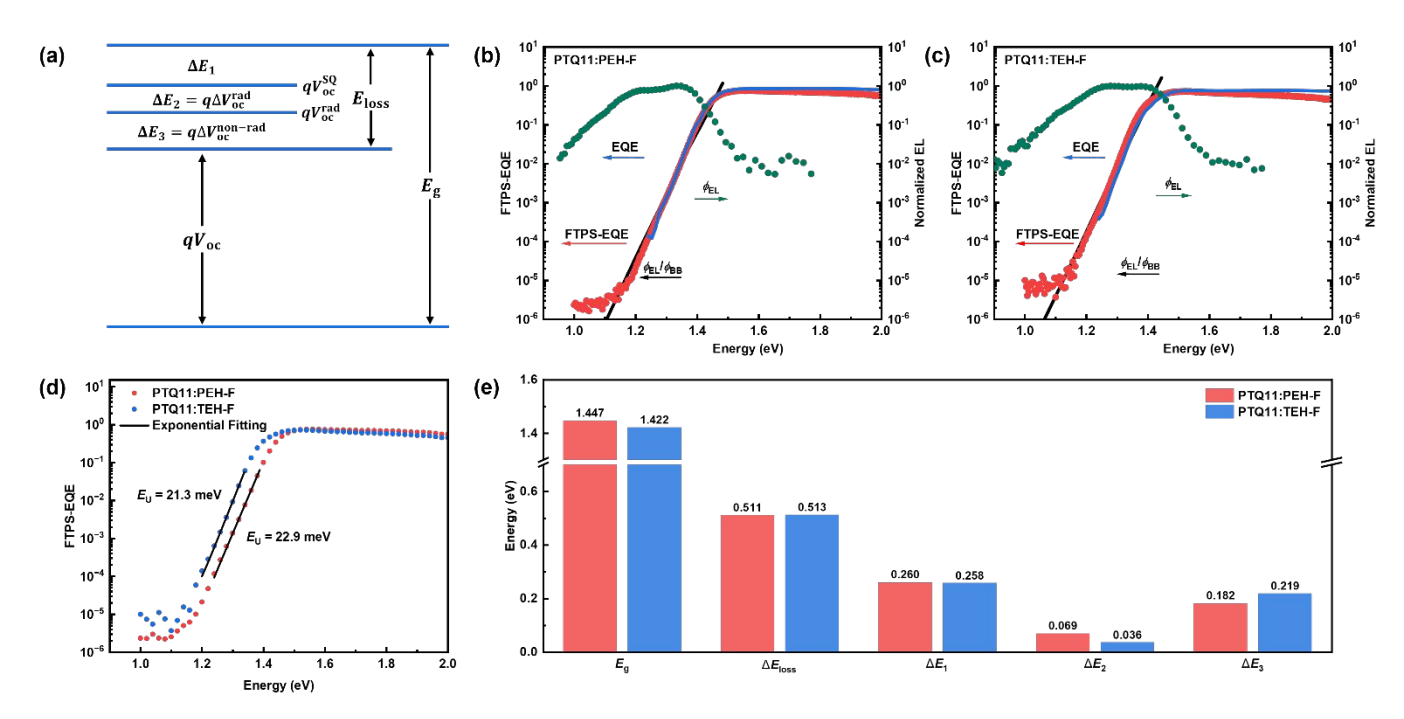


Fig. 2 (a) Schematic diagram for V_{loss}/E_{loss} of OSCs according to the SQ limit. Semilogarithmic plots of normalized electroluminescence (EL), measured EQE, and FTPS-EQE spectra as a function of energy for devices based on (b) PTQ11:PEH-F and (c) PTQ11:TEH-F. The ratio of ϕ_{EL}/ϕ_{bb} was used to plot the EQE in the low-energy regime, where ϕ_{EL} and ϕ_{bb} represent the emitted photon flux and the room-temperature blackbody photon flux, respectively. (d) The calculation of E_U for devices based on PTQ11:PEH-F and PTQ11:TEH-F. e) E_g , E_{loss} and its detailed three components of ΔE_1 , ΔE_2 , and ΔE_3 for devices based on PTQ11:PEH-F and PTQ11:TEH-F.

Exciton Dissociation and Charge Carrier Recombination

Exciton dissociation and charge carrier recombination are crucial processes that determines the charge generation of OSCs, thus significantly affects the photovoltaic performance of the devices. As mentioned above, the exciton dissociation in PTQ11:PEH-F blend may be restricted due to the weak driving force for hole transfer because of the small ΔE_{HOMO} value (0.06 eV) between PTQ11 and PEH-F. Therefore, for investigating the exciton dissociation and charge carrier recombination in the OSCs based on PTQ11:PEH-F and PTQ11:TEH-F, we measured the dependence of photocurrent density (J_{ph}) on the effective voltage ($V_{\rm eff}$), and the dependence of $V_{\rm oc}$ and $J_{\rm sc}$ on the light intensity (P_{light}). From the dependence of J_{ph} on V_{eff} of the devices (Fig. S8a), it is found that the PTQ11:PEH-F-based device possess more efficient exciton dissociation and charge collection processes with higher exciton dissociation probabilities (P_{diss}) and charge collection probabilities (P_{coll}) than that of the PTQ11:TEH-F-based device (the details are depicted after Fig. S7), which could contribute to higher J_{sc} and FF.⁴⁹ Fig. 3a and Fig. S8b shows the plots of $V_{\rm oc}$ vs. In $P_{\rm light}$ for the OSCs, in which the slope of the fitting lines should be nkT/q(1<n<2, where k, T, and q denote Boltzmann constant, Kelvin temperature and elementary charge, respectively.).50 When the value of n is close to 2 means that trap-assisted recombination dominates, whereas when the value of *n* is close to 1 means that bimolecular recombination dominates. The average slopes for the devices based on PTQ11:PEH-F and PTQ11:TEH-F are 1.19 kT/q and 1.33 kT/q respectively, which indicates that the major charge recombination mechanism for both OSCs should be bimolecular recombination and more severe trap-assisted recombination occurs in PTQ11:TEH-F blend. Fig. 3b and Fig. S8b illustrates the plots of log $J_{\rm sc}$ vs. log $P_{\rm light}$, and the relationship of $J_{\rm sc}$ and $P_{\rm light}$ can be described as $J_{\rm sc} \propto (P_{\rm light})^{\alpha}$, where α indicates the degree of bimolecular recombination. The closer the α value is to 1, the weaker the bimolecular recombination exists in the active layer. The average α values determined from the slopes of log $J_{\rm sc}$ vs. log $P_{\rm light}$ are 0.996 for the PTQ11:PEH-F based OSC and 0.977 for the PTQ11:TEH-F based OSC, indicating there is less bimolecular recombination in the former.

In addition, to study the overall process of charge carrier generation, transport, and extraction of the OSCs in working condition under illumination, we measured transient photocurrent (TPC) and photon-induced charge-carrier extraction in linearly increasing voltage (photo-CELIV) of two devices. As shown in Fig. 3c, the PEH-F-based OSC displays faster turn-on and turn-off dynamic compared to the TEH-F-based OSC, which implies that there are rapid charge generation/extraction and less trapped charge in the former device. Fig. S8c displays the transient signal of photo-CELIV, and the carrier extraction mobilities obtained from the photo-CELIV measurement are 2.78 × 10⁻⁴ cm² V⁻¹ s⁻¹ and 2.19 × 10⁻⁴ cm² V⁻¹ s⁻¹ for the OSCs based on PTQ11:PEH-F and PTQ11:TEH-F, respectively. Consequently, these results above suggest that the PTQ11:PEH-F based OSC possesses more efficient charge

generation/extraction and carrier transport, which is beneficial to realize superior Jsc and FF in the devices.

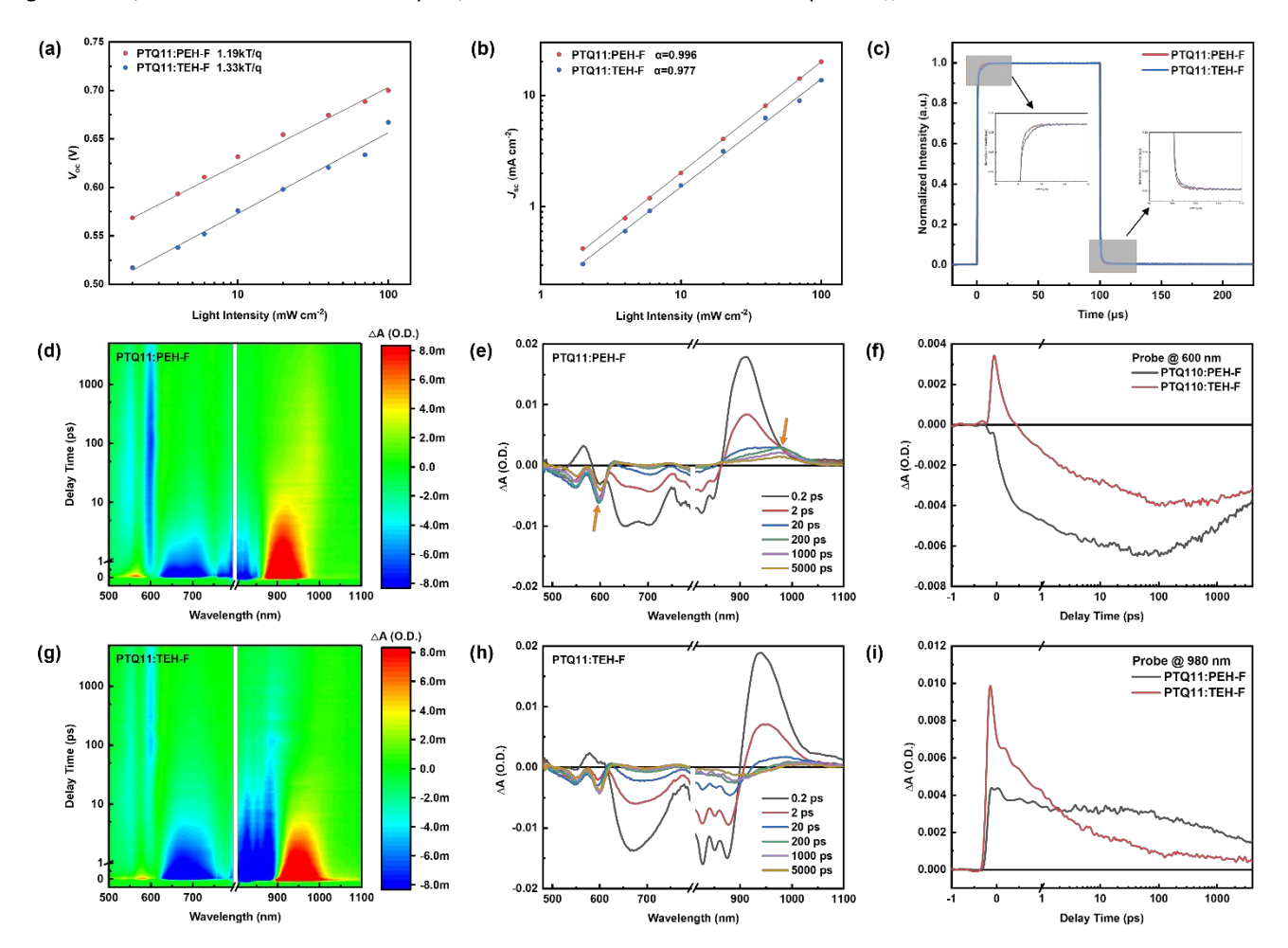


Fig. 3 (a) Plots of V_{oc} vs. In P_{light} of the optimized OSCs. (b) Plots of log J_{sc} vs. log P_{light} of the optimized OSCs. (c) Normalized TPC in response to a 100 μ s white light (LED) pulse of the optimized OSCs. 2D femtosecond transient absorption spectra of (d) PTQ11:PEH-F blend film and (g) PTQ11:TEH-F blend film. Transient absorption spectra profiles of (e) PTQ11:PEH-F blend film and (h) PTQ11:TEH-F blend film at selective delay times. (f) Kinetic traces of the donor GSB probing at 600 nm for PTQ11:PEH-F blend film (black) and PTQ11:TEH-F blend film (red). (i) Kinetic traces of CT state probing at 980 nm for PTQ11:PEH-F blend film (black) and PTQ11:TEH-F blend film (red).

Charge Transfer Dynamics

Generally, the photoactive layer materials of OSCs absorb photons to generate excitons, and the excitons diffuse to the donor/acceptor interface in the presence of a concentration gradient and then dissociate under an extra driving force to form a CT state electron-hole pair with electron in the LUMO of acceptor and hole in the HOMO of donor. After that, the electron-hole pair could further effectively dissociate into free charge carriers, thus contributing to the photocurrents. $^{31,52-54}$ As for the driving force, it is empirically considered to derive from the frontier molecular orbital energy offsets between donor and acceptor (including the $\Delta E_{\rm HOMO(D-A)}$ and $\Delta E_{\rm LUMO(D-A)}$), and it is believed that sufficient frontier orbital energy offsets is necessary for driving the exciton dissociation and CT.

In surprise, as mentioned above, it seems that the PTQ11:PEH-F blend possesses more efficient exciton dissociation and CT even though it theoretically has a smaller driving force for hole transfer due to the smaller $\Delta E_{\text{HOMO}(D\text{-A})}$

value of only 0.06 eV. Here, we employed the broadband femtosecond transient absorption (fs-TA) spectroscopy measurement for acceptor pristine films and blend films to obtain a better insight into the CT dynamic and the carrier recombination processes in the active layers. For the pristine films, two acceptors exhibit similar spectral profiles, i.e., excited state absorption (ESA) peaks at around 560 nm and 920 nm, and ground state bleach (GSB) peaks at around 650 nm and 850 nm (Fig. S9). For the blend films, as depicted in Fig. 3e and 3h, the spectrums are predominated by the excited state signals of acceptors within the first 0.2 ps after excitation, which is consistent with the spectrums of the acceptor pristine films. After the fast CT process occurs, the excited state signals of acceptors decay rapidly within 20 ps with new TA signals appear, including the GSB peaks of donor at around 540 nm and 600 nm, and a new ESA peak of acceptors at around 980 nm. Notably, the intensities of the characteristic TA peaks of PTQ11:PEH-F blend at around 600 nm and 980 nm are

significantly higher than those of PTQ11:TEH-F blend film (as shown in Fig. 3e, marked by the orange arrows), indicating that the former achieves a greater CT state yield even at a smaller $\Delta E_{\text{HOMO}(D-A)}$ value of 0.06 eV, which is also corroborated by the kinetic traces of the donor GSB at 600 nm (Fig. 3f). Meanwhile, the slower decay rate of the ESA peak at 980 nm for PTQ11:PEH-F blend suggests that there is less charge recombination from the CT state to the ground state in the film, and it has a longer nanosecond charge carrier lifetime (as

displayed in Fig. 3i, the PTQ11:TEH-F blend film has a stronger intensity at the beginning because of its ESA signal in the CT state partially overlaps with the ESA signal in the acceptor excited state). On balance, higher CT state yield and less charge recombination in PTQ11:PEH-F blend film imply more efficient exciton dissociation and hole transfer processes even at small $\Delta E_{\rm HOMO(D-A)}$ of 0.06 eV, resulting in better photovoltaic performance for the devices.

Microscopic Morphology

To further explore the effect of conjugated outer side chain on the molecular self-assembly and aggregation features, as well as the micro-nano texture of blend photoactive layer, the thinfilm microscopic morphology of donor and acceptors pristine and blend films were investigated by grazing incidence wideangle X-ray scattering (GIWAXS), as shown in Fig. 4 and Fig. S10. PTQ11 and two SMAs pristine films illustrate the dominant face-on orientation, and the (010) diffraction peaks of PEH-F and TEH-F pristine films in the out-of-plane (OOP) direction are located at 1.700 Å⁻¹ (*d*-spacing: 3.695 Å) and 1.739 Å⁻¹ (*d*spacing: 3.611 Å), respectively. By means of the Scherrer equation in reciprocal space, the crystal coherence lengths (CCLs) of $\pi\text{-}\pi$ stacking are estimated to be 11.7 Å for PEH-F and 14.3 Å for TEH-F from the full width at half maximum (FWHM) of the diffraction peaks, as tabulated in Table S17. The closer π - $\boldsymbol{\pi}$ stacking and longer CCL in the OOP direction of TEH-F pristine film reveal that the thienyl outer side chains lead to stronger and more ordered intermolecular packing of molecule than the phenyl outer side chains. After blending with the polymer donor PTQ11, the CCLs of $\pi\text{-}\pi$ stacking in the OOP direction for the PTQ11:PEH-F and PTQ11:TEH-F blend films increase to 18.0 Å and 19.2 Å, respectively. However, it is noteworthy that two new lamellar diffraction peaks with molecular edge-on stacking orientation are observed at 0.614 $\mbox{\normalfont\AA}^{-1}$ and 1.510 $\mbox{\normalfont\AA}^{-1}$ in the OOP direction in PTQ11:TEH-F blend film (as shown in Fig. 4d, marked by the orange arrows), indicating that the addition of PTQ11 disrupts the original aggregation of TEH-F and induces a shift of molecular orientation from face-on to edge-on, which is not conductive for the charge transport in the blend. In order to gain a deeper insight into the effect of different conjugated outer side chains on the charge transport properties in the photoactive layer, we measured the hole (μ_h) and electron (μ_e) mobilities of two blend films by the space charge limited current (SCLC) method, and the results are shown in Fig. S11 and Table S18. It can be seen that the PTQ11:PEH-F blend film shows higher and more balanced μ_h and μ_e values (7.51 \times 10 $^{4}/8.34 \times 10^{-4} \text{ cm}^{2} \text{ V}^{-1} \text{ s}^{-1}$) with μ_{h}/μ_{e} ratio of 0.90 than that (6.52 $\times\,10^{\text{-4}}/8.25\times10^{\text{-4}}~\text{cm}^{\text{2}}~\text{V}^{\text{-1}}~\text{s}^{\text{-1}})$ of the PTQ11:TEH-F blend film with μ_h/μ_e ratio of 0.79, which could facilitate the charge transport and deliver better FF in the PTQ11:PEH-F-based OSCs.

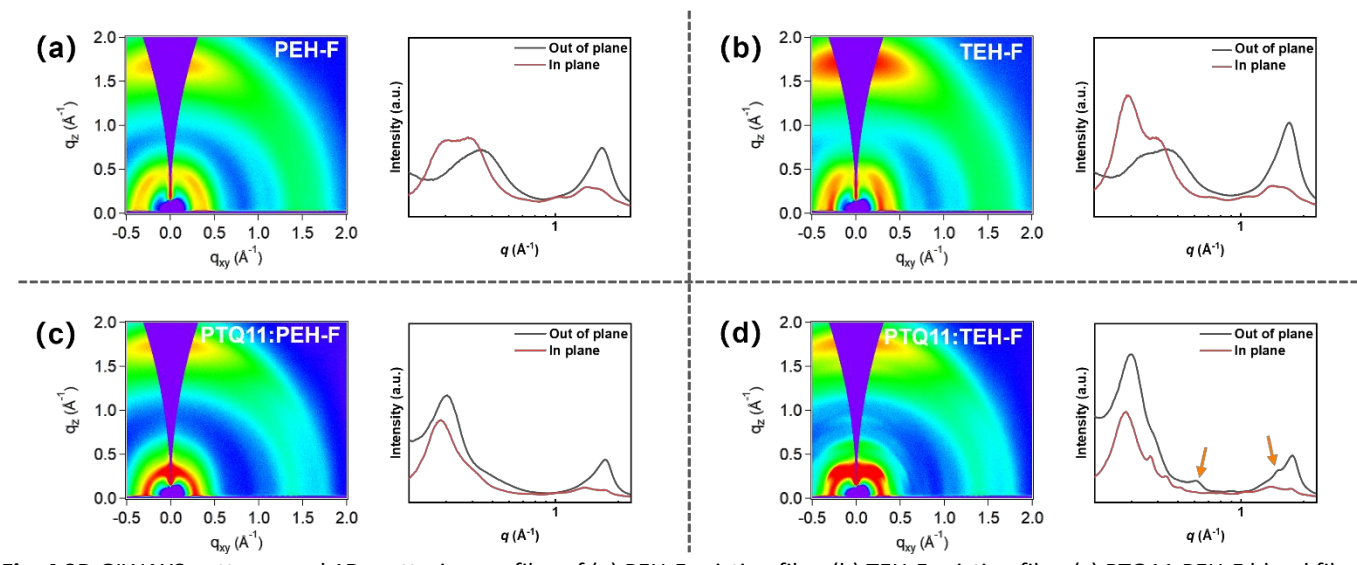


Fig. 4 2D GIWAXS patterns and 1D scattering profiles of (a) PEH-F pristine film, (b) TEH-F pristine film, (c) PTQ11:PEH-F blend film, and (d) PTQ11:TEH-F blend film.

Cost Feasibility of Solar Modules

Cost of solar modules is the critical parameter to determine the industrialization potential and application competitiveness of photovoltaic technology. 55-56 Given the outstanding photovoltaic performance and the low-cost characteristic of polymer PTQ11, the PTQ11:PEH-F-based OSC is expected to

have high cost feasibility for industrialization. In this section, we evaluate the cost feasibility of PTQ11:PEH-F-based OSC by minimum sustainable price (MSP) of module, which is widely used in the cost analysis of photovoltaic technologies.^{27-28,57-60} Typically, the MSP of photovoltaics could be expressed as the following equation (3):

$$MSP = (MC + OH + WACC) / (I \times PCE \times GFF)$$
 (3)

Wherein, MC represents the manufacturing cost of solar module, including the costs of raw materials (such as photoactive materials, electrodes, electrode buffer layer materials, solvents, glass, barrier foil, and sealant, etc.), utilities (including electricity and water), labors, maintenance and depreciation of the equipment and buildings. OH represents the overhead cost associated with the manufacturing process (such as the costs of scales, general, and administrative (SG&A), research and development (R&D), and taxes and interest). WACC represents the weighted average cost of capital. "I" represents the solar irradiance power density, assumed to be AM 1.5G, 1000 W m⁻². PCE is the power conversion efficiency of solar module. GFF represents the geometric fill factor of solar module, i.e., the ratio of sunlight utilization area to the processing area, which is assumed to be 98% here. Therefore, reducing the cost of photoactive materials and/or increasing the PCE of devices are viable methods to achieve low MSP for solar modules.

On the basis of the same costing protocol of acceptors PEH-F and TEH-F mentioned in the "Molecular Synthesis and Characterization" section and "Cost Feasibility of Organic Photovoltaic Materials" section (ESI), we also calculate the $C_{\rm kg}$ of reported high-performance SMAs (m-TEH, BTP-4F-P2EH, BTP-ec9, and L8-BO) and polymer donors (PTQ11, PTQ10, PM6, D18, and D18-Cl) to assess the cost feasibility of the highperformance OSCs systems for industrialization (as shown in Fig. 5a and Table S5-S15). It is found that the $C_{\rm kg}$ of PEH-F $(234.74 \times 10^3 \ \text{kg}^{-1})$ is slightly higher than that of BTP-eC9 (215.14 \times 10³ \$ kg⁻¹), but significantly lower than that of *m*-TEH $(264.56 \times 10^{3} \text{ $ kg}^{-1})$ and L8-BO $(271.84 \times 10^{3} \text{ $ kg}^{-1})$. The main reason for this difference is the synthesis cost of these molecules caused by the different cost of halogenated end groups, that is, the cost of monofluorine-substituted and dichloro-substituted end groups is lower than that of bifluorinesubstituted end group. For polymer donors, PTQ11 exhibits an impressively lowest C_{kg} of 33.70 \times 10³ \$ kg⁻¹, only

approximately one-fifth to one-sixth of "star" highperformance polymer donors PM6, D18, and D18-Cl. Thus, we believe that the PTQ11:PEH-F-based OSCs are highly costfeasible for industrialization. Then, to explore this inference, we calculate the MSP of PTQ11:PEH-F based OSC and other reported high-performance OSCs with PCEs over 19%, based on the industrial sub-device architecture and processing technologies of solar modules with some reasonable assumptions (Fig. S12, and Table S19-20). As displayed in Fig. 5b and Table S21, the PTQ11:PEH-F based OSC delivers the lowest cost of photoactive layer materials (32.25 \$ m⁻²), and thus the lowest MC + OH + WACC value (67.99 \$ m⁻²) among the statistical twenty-two photoactive layer systems. Furthermore, benefiting from the superior photovoltaic performance, the PTQ11:PEH-F-based OSC exhibits the lowest MSP of 0.35 $$W_p^-$$ ¹ (cost-per-peak-Watt), which is dramatically lower than that of other reported high-performance OSCs which generally possess high MSP of exceeding 0.42 $\$ W_p^{-1} (as illustrated in Fig. 5C and Table S21). To the best of our knowledge, the MSP of 0.35 $$W_p^-$$ ¹ for PTQ11:PEH-F-based OSC is the minimum value reported to date for organic photovoltaics. Hence, it is believed that PTQ11:PEH-F-based binary device with small efficiency-cost gap is highly promising for future large-area fabrication and commercial application of OSCs. More importantly, the variable molecular structures and synthetic routes of organic photovoltaic materials gives OSCs great potential for realizing low cost and high efficiency simultaneously, which could considerably reduce the MSP of OSC modules. Based on the calculation results of our cost feasibility analysis, we find that the complex molecular structure of A-DA'D-A type SMAs results in significantly higher synthesis cost and isolation/purification cost than those of PTQ-series polymer donors (as displayed in Fig.5a), which greatly hampers the further reduction of MSP for OSC modules. Therefore, there is an urgent need to develop high-performance acceptor materials with simple structure and low cost, thus conferring great prospect and competitiveness of OSCs for commercial application in the future.

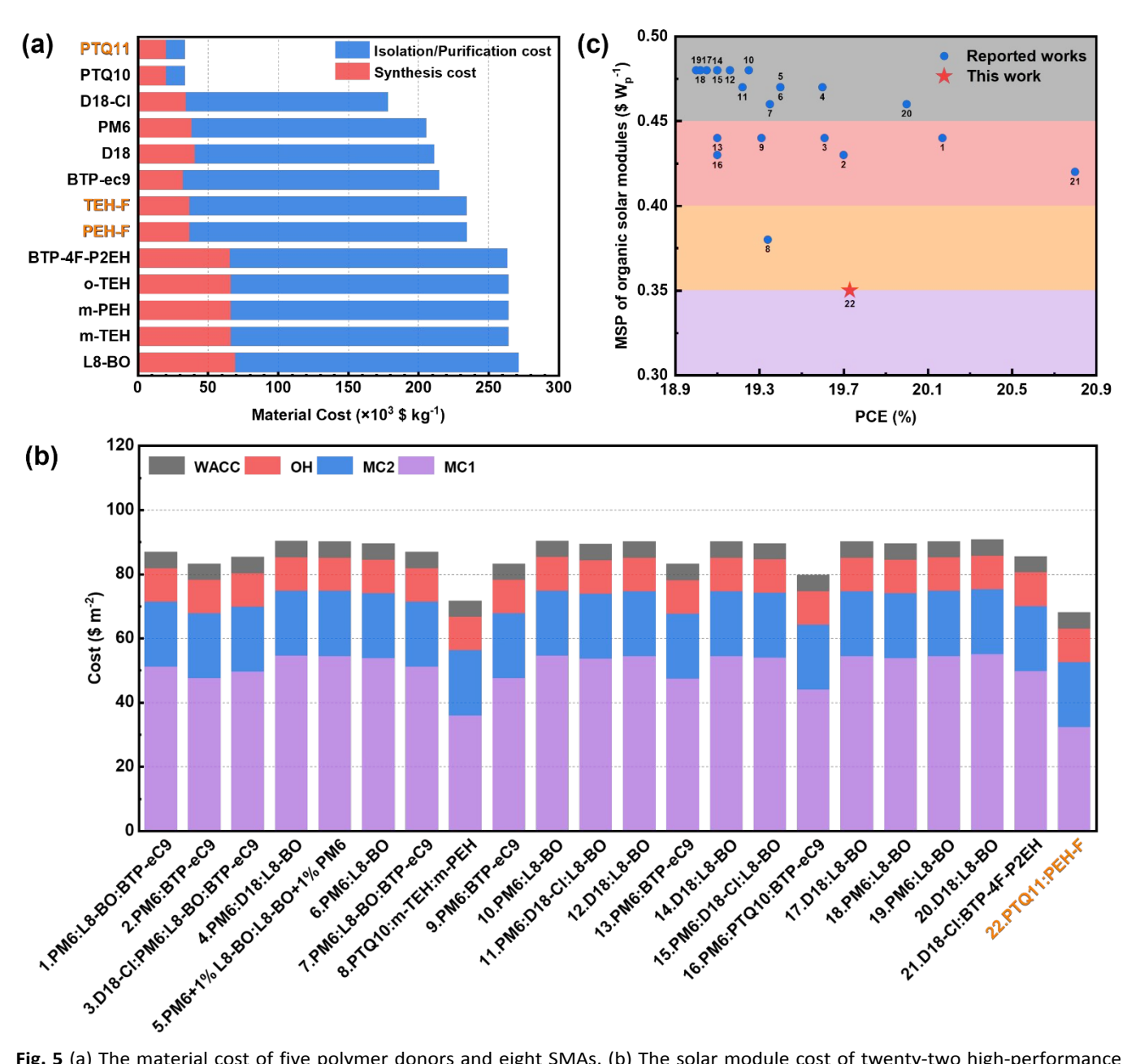


Fig. 5 (a) The material cost of five polymer donors and eight SMAs. (b) The solar module cost of twenty-two high-performance OSCs systems (MC1 refers to the photoactive layer cost). (c) The MSP of twenty-two high-performance organic solar modules.

Conclusions

In summary, two SMAs with different bulky conjugated outer side chains, namely PEH-F and TEH-F, were rationally designed and synthesized, and the impacts of the different outer side chains on their optoelectronic and molecular aggregation properties were investigated. Compared to TEH-F with thienyl outer side chain, PEH-F with phenyl outer side chain exhibits wider $E_{\rm g}^{\rm opt}$, slightly up-shifted frontier energy levels, and higher absorption coefficient. By employing the low-cost polymer PTQ11 as donor, the OSC based on PEH-F shows low $E_{\rm loss}$ of 0.511 eV owing to the suppressed non-radiative loss of only

0.182 eV, and efficient exciton dissociation and hole transfer processes even at an extremely small $\Delta E_{\rm HOMO~(D-A)}$ of only 0.06 eV, thus yielding an outstanding PCE of 19.73 % with a high $V_{\rm oc}$ of 0.936 V and a large $J_{\rm sc}$ of 26.53 mA cm $^{-2}$ simultaneously. As far as we know, 19.73% is the highest PCE of OSCs based on the low-cost polymers to date. More importantly, the PTQ11:PEH-F-based device shows satisfactory cost feasibility for industrialization with the estimated MSP of only 0.35 \$ Wp $^{-1}$, which is dramatically lower than other reported high-performance OSCs. These results implying that the PTQ11:PEH-F binary system is a promising candidate with small efficiency-cost gap for industrial organic photovoltaic.

Author contributions

X. K. and C. S. conceived the idea, designed the experiments and supervised the project. X. K. carried out the synthesis experiments and wrote the initial draft. N. Y. performed the fabrication, measurement, and analysis of the devices. X. Z. and A.L. helped in synthesizing the photoactive materials. J. Z. and J. L. conducted the TA measurements and data analysis. Z. L., X. L. and G.Y. assisted in analyzing the cost feasibility of solar modules. Y. W. conducted the GIWAXS measurements and data analysis. R. S. and J. M. conducted the V_{loss}/E_{loss} measurements and data analysis. All authors discussed and commented on the manuscript.

Conflicts of interest

There are no conflicts to declare.

Data availability

The data that support the findings of this study are available in the supplementary material of this article.

Acknowledgements

This work was supported by the National Natural Science Foundation of China (Nos. 52103240 and 52103243), the Natural Science Foundation of Henan (No. 212300410284). GIWAXS measurement was carried out at the Stanford Synchrotron Radiation Laboratory (SSRL), SLAC National Accelerator Laboratory, supported by the U.S. Department of Energy, Office of Basic Energy Sciences under Contract No. DE-AC02-76SF00515.

Notes and references

- S. Karuthedath, J. Gorenflot, Y. Firdaus, N. Chaturvedi, C. S. P. De Castro, G. T. Harrison, J. I. Khan, A. Markina, A. H. Balawi, T. A. D. Peña, W. Liu, R.-Z. Liang, A. Sharma, S. H. K. Paleti, W. Zhang, Y. Lin, E. Alarousu, D. H. Anjum, P. M. Beaujuge, S. De Wolf, I. McCulloch, T. D. Anthopoulos, D. Baran, D. Andrienko and F. Laquai, *Nat. Mater.*, 2021, 20, 378–384.
- 2 D. Meng, R. Zheng, Y. Zhao, E. Zhang, L. Dou and Y. Yang, *Adv. Mater.*, 2022, **34**, 2107330.
- 3 Q. Shen, C. He, S. Li, L. Zuo, M. Shi and H. Chen, Acc. Mater. Res., 2022, 3, 644–657.
- 4 H. Yao and J. Hou, *Angew. Chem. Int. Ed.*, 2022, **61**, e202209021.
- 5 G. Zhang, F. R. Lin, F. Qi, T. Heumüller, A. Distler, H.-J. Egelhaaf, N. Li, P. C. Y. Chow, C. J. Brabec, A. K.-Y. Jen and H.-L. Yip, *Chem. Rev.*, 2022, **122**, 14180–14274.
- 6 J. Wang, P. Xue, Y. Jiang, Y. Huo and X. Zhan, *Nat. Rev. Chem.*, 2022, **6**, 614–634.
- 7 J. Yi, G. Zhang, H. Yu and H. Yan, *Nat. Rev. Mater.*, 2023, **9**, 46–62.

- P. Ding, D. Yang, S. Yang and Z. Ge, Chem. Soc. Rev., 2024, 53, 2350–2387.
- M. Zhang, X. Guo, W. Ma, H. Ade and J. Hou, *Adv. Mater.*, 2015, 27, 4655–4660.
- 10 C. Sun, F. Pan, H. Bin, J. Zhang, L. Xue, B. Qiu, Z. Wei, Z.-G. Zhang and Y. Li, *Nat. Commun.*, 2018, 9, 743.
- 11 Q. Liu, Y. Jiang, K. Jin, J. Qin, J. Xu, W. Li, J. Xiong, J. Liu, Z. Xiao, K. Sun, S. Yang, X. Zhang and L. Ding, *Sci. Bull.*, 2020, 65, 272–275.
- 12 J. Qin, L. Zhang, C. Zuo, Z. Xiao, Y. Yuan, S. Yang, F. Hao, M. Cheng, K. Sun, Q. Bao, Z. Bin, Z. Jin and L. Ding, *J. Semicond.*, 2021, **42**, 010501.
- 13 J. Yuan, Y. Zhang, L. Zhou, G. Zhang, H.-L. Yip, T.-K. Lau, X. Lu, C. Zhu, H. Peng, P. A. Johnson, M. Leclerc, Y. Cao, J. Ulanski, Y. Li and Y. Zou, *Joule*, 2019, 3, 1140–1151.
- 14 Y. Cui, H. Yao, J. Zhang, K. Xian, T. Zhang, L. Hong, Y. Wang, Y. Xu, K. Ma, C. An, C. He, Z. Wei, F. Gao and J. Hou, Adv. Mater., 2020, 32, 1908205.
- C. Li, J. Zhou, J. Song, J. Xu, H. Zhang, X. Zhang, J. Guo, L. Zhu,
 D. Wei, G. Han, J. Min, Y. Zhang, Z. Xie, Y. Yi, H. Yan, F. Gao,
 F. Liu and Y. Sun, *Nat. Energy*, 2021, 6, 605–613.
- 16 J. Fu, Q. Yang, P. Huang, S. Chung, K. Cho, Z. Kan, H. Liu, X. Lu, Y. Lang, H. Lai, F. He, P. W. K. Fong, S. Lu, Y. Yang, Z. Xiao and G. Li, *Nat. Commun.*, 2024, **15**, 1830.
- 17 J. Huang, T. Chen, L. Mei, M. Wang, Y. Zhu, J. Cui, Y. Ouyang, Y. Pan, Z. Bi, W. Ma, Z. Ma, H. Zhu, C. Zhang, X.-K. Chen, H. Chen and L. Zuo, *Nat. Commun.*, 2024, **15**, 3287.
- 18 J. Yao, B. Qiu, Z.-G. Zhang, L. Xue, R. Wang, C. Zhang, S. Chen, Q. Zhou, C. Sun, C. Yang, M. Xiao, L. Meng and Y. Li, *Nat. Commun.*, 2020, 11, 2726.
- 19 Y. Yang, J. Wang, Y. Zu, Q. Liao, S. Zhang, Z. Zheng, B. Xu and J. Hou, *Joule*, 2023, **7**, 545–557.
- 20 J. Yao, S. Ding, R. Zhang, Y. Bai, Q. Zhou, L. Meng, E. Solano, J. A. Steele, M. B. J. Roeffaers, F. Gao, Z. Zhang and Y. Li, *Adv. Mater.*, 2022, **34**, 2203690.
- 21 Y. Yu, J. Wang, Y. Cui, Z. Chen, T. Zhang, Y. Xiao, W. Wang, J. Wang, X.-T. Hao and J. Hou, J. Am. Chem. Soc., 2024, 146, 8697–8705
- 22 L. Zhu, M. Zhang, J. Xu, C. Li, J. Yan, G. Zhou, W. Zhong, T. Hao, J. Song, X. Xue, Z. Zhou, R. Zeng, H. Zhu, C.-C. Chen, R. C. I. MacKenzie, Y. Zou, J. Nelson, Y. Zhang, Y. Sun and F. Liu, Nat. Mater., 2022, 21, 656–663.
- R. Sun, T. Wang, X. Yang, Y. Wu, Y. Wang, Q. Wu, M. Zhang,
 C. J. Brabec, Y. Li and J. Min, *Nat. Energy*, 2022, 7, 1087–
- 24 J. Fu, P. W. K. Fong, H. Liu, C.-S. Huang, X. Lu, S. Lu, M. Abdelsamie, T. Kodalle, C. M. Sutter-Fella, Y. Yang and G. Li, *Nat. Commun.*, 2023, **14**, 1760.
- 25 Y. Zhang, W. Deng, C. E. Petoukhoff, X. Xia, Y. Lang, H. Xia, H. Tang, H. T. Chandran, S. Mahadevan, K. Liu, P. W. K. Fong, Y. Luo, J. Wu, S.-W. Tsang, F. Laquai, H. Wu, X. Lu, Y. Yang and G. Li, *Joule*, 2024, **8**, 509–526.
- 26 K. Jiang, Q. Wei, J. Y. L. Lai, Z. Peng, H. K. Kim, J. Yuan, L. Ye, H. Ade, Y. Zou and H. Yan, *Joule*, 2019, **3**, 3020–3033.
- 27 J. Guo and J. Min, Adv. Energy Mater., 2019, 9, 1802521.

- 28 W. Yang, W. Wang, Y. Wang, R. Sun, J. Guo, H. Li, M. Shi, J. Guo, Y. Wu, T. Wang, G. Lu, C. J. Brabec, Y. Li and J. Min, *Joule*, 2021, 5, 1209–1230.
- 29 K. Chong, X. Xu, H. Meng, J. Xue, L. Yu, W. Ma and Q. Peng, *Adv. Mater.*, 2022, **34**, 2109516.
- 30 L. Tu, H. Wang, W. Duan, R. Ma, T. Jia, T. A. Dela Peña, Y. Luo, J. Wu, M. Li, X. Xia, S. Wu, K. Chen, Y. Wu, Y. Huang, K. Yang, G. Li and Y. Shi, *Energy Environ. Sci.*, 2024, 17, 3365–3374.
- 31 C. Sun, S. Qin, R. Wang, S. Chen, F. Pan, B. Qiu, Z. Shang, L. Meng, C. Zhang, M. Xiao, C. Yang and Y. Li, *J. Am. Chem. Soc.*, 2020, 142, 1465–1474.
- 32 Y. Wang, D. Qian, Y. Cui, H. Zhang, J. Hou, K. Vandewal, T. Kirchartz and F. Gao, *Adv. Energy Mater.*, 2018, **8**, 1801352.
- 33 A. J. Gillett, A. Privitera, R. Dilmurat, A. Karki, D. Qian, A. Pershin, G. Londi, W. K. Myers, J. Lee, J. Yuan, S.-J. Ko, M. K. Riede, F. Gao, G. C. Bazan, A. Rao, T.-Q. Nguyen, D. Beljonne and R. H. Friend, *Nature*, 2021, **597**, 666–671.
- 34 S. Liu, J. Yuan, W. Deng, M. Luo, Y. Xie, Q. Liang, Y. Zou, Z. He, H. Wu and Y. Cao, *Nat. Photonics*, 2020, **14**, 300–305.
- 35 Y. Wang, J. Yu, R. Zhang, J. Yuan, S. Hultmark, C. E. Johnson, N. P. Gallop, B. Siegmund, D. Qian, H. Zhang, Y. Zou, M. Kemerink, A. A. Bakulin, C. Müller, K. Vandewal, X.-K. Chen and F. Gao, *Nat. Energy*, 2023, **8**, 978–988.
- 36 Y. Shi, Y. Chang, K. Lu, Z. Chen, J. Zhang, Y. Yan, D. Qiu, Y. Liu, M. A. Adil, W. Ma, X. Hao, L. Zhu and Z. Wei, *Nat. Commun.*, 2022, 13, 3256.
- 37 L. Zhan, S. Li, Y. Li, R. Sun, J. Min, Z. Bi, W. Ma, Z. Chen, G. Zhou, H. Zhu, M. Shi, L. Zuo and H. Chen, *Joule*, 2022, 6, 662–675.
- 38 K. Liu, Y. Jiang, G. Ran, F. Liu, W. Zhang and X. Zhu, *Joule*, 2024, **8**, 835–851.
- 39 H. Chen, H. Liang, Z. Guo, Y. Zhu, Z. Zhang, Z. Li, X. Cao, H. Wang, W. Feng, Y. Zou, L. Meng, X. Xu, B. Kan, C. Li, Z. Yao, X. Wan, Z. Ma and Y. Chen, *Angew. Chem. Int. Ed.*, 2022, 61, e202209580.
- 40 K. Jiang, J. Zhang, C. Zhong, F. R. Lin, F. Qi, Q. Li, Z. Peng, W. Kaminsky, S.-H. Jang, J. Yu, X. Deng, H. Hu, D. Shen, F. Gao, H. Ade, M. Xiao, C. Zhang and A. K.-Y. Jen, *Nat Energy*, 2022, 7, 1076–1086.
- 41 G. Chai, Y. Chang, J. Zhang, X. Xu, L. Yu, X. Zou, X. Li, Y. Chen, S. Luo, B. Liu, F. Bai, Z. Luo, H. Yu, J. Liang, T. Liu, K. S. Wong, H. Zhou, Q. Peng and H. Yan, *Energy Environ. Sci.*, 2021, 14, 3469–3479.

- 42 X. Kong, C. Zhu, J. Zhang, L. Meng, S. Qin, J. Zhang, J. Li, Z. Wei and Y. Li, *Energy Environ. Sci.*, 2022, **15**, 2011–2020.
- 43 X. Kong, J. Zhang, L. Meng, C. Sun, S. Qin, C. Zhu, J. Zhang, J. Li, Z. Wei and Y. Li, *CCS Chem.*, 2023, **5**, 841–850.
- 44 X. Wu, X. Zhang, J. Zhang, Y. Wu, J. Li, X. Kong, Z. Li, X. Zhang, X. Li, A. Li, G. Yang and C. Sun, *Adv. Funct. Mater.*, 2024, 2405168.
- 45 J. Yao, T. Kirchartz, M. S. Vezie, M. A. Faist, W. Gong, Z. He, H. Wu, J. Troughton, T. Watson, D. Bryant and J. Nelson, *Phys. Rev. Appl.*, 2015, 4, 014020.
- 46 C. Kaiser, O. J. Sandberg, N. Zarrabi, W. Li, P. Meredith and A. Armin, *Nat. Commun.*, 2021, **12**, 3988.
- 47 N. K. Elumalai and A. Uddin, *Energy Environ. Sci.*, 2016, **9**, 391–410.
- 48 R. Wang, J. Xu, L. Fu, C. Zhang, Q. Li, J. Yao, X. Li, C. Sun, Z.-G. Zhang, X. Wang, Y. Li, J. Ma and M. Xiao, *J. Am. Chem. Soc.*, 2021, **143**, 4359–4366.
- 49 S. R. Cowan, A. Roy and A. J. Heeger, *Phys. Rev. B*, 2010, **82**, 245207.
- 50 L. J. A. Koster, M. Kemerink, M. M. Wienk, K. Maturová and R. A. J. Janssen, *Adv. Mater.*, 2011, **23**, 1670–1674.
- L. Hong, H. Yao, Z. Wu, Y. Cui, T. Zhang, Y. Xu, R. Yu, Q. Liao,
 B. Gao, K. Xian, H. Y. Woo, Z. Ge and J. Hou, *Adv. Mater.*,
 2019, 31, 1903441.
- 52 A. Tang, B. Xiao, Y. Wang, F. Gao, K. Tajima, H. Bin, Z. Zhang, Y. Li, Z. Wei and E. Zhou, *Adv. Funct. Mater.*, 2018, 28, 1704507.
- 53 L. Zhu, J. Zhang, Y. Guo, C. Yang, Y. Yi and Z. Wei, *Angew. Chem. Int. Ed.*, 2021, **60**, 15348–15353.
- 54 G. Han and Y. Yi, Acc. Chem. Res., 2022, 55, 869–877.
- 55 B. Lee, L. Lahann, Y. Li and S. R. Forrest, *Sustainable Energy Fuels*, 2020, **4**, 5765–5772.
- 56 Y. Li, X. Huang, H. K. M. Sheriff and S. R. Forrest, *Nat. Rev. Mater.*, 2022, 8, 186–201.
- 57 B. Azzopardi, C. J. M. Emmott, A. Urbina, F. C. Krebs, J. Mutale and J. Nelson, *Energy Environ. Sci.*, 2011, **4**, 3741.
- 58 C. J. M. Emmott, A. Urbina and J. Nelson, *Solar Energy Materials and Solar Cells*, 2012, **97**, 14–21.
- 59 T. P. Osedach, T. L. Andrew and V. Bulović, *Energy Environ. Sci.*, 2013, **6**, 711.
- 60 A. Gambhir, P. Sandwell and J. Nelson, *Solar Energy Materials and Solar Cells*, 2016, **156**, 49–58.

Data Availability Statement

The data supporting this article have been included as part of the Supplementary Information.